Appl. Phys. A (2016)122:138
DOI 10.1007/s00339-016-9677-7

Applied Physics A
Materials Science & Processing

Simulation and optimization of current matching double-junction InGaN/Si solar cells

S. Nacer[1] · A. Aissat[1]

Received: 4 November 2015 / Accepted: 28 January 2016

Abstract This paper deals with theoretical investigation of the performance of current-matched In_xGaN/Si double-junction solar cells. Calculations were performed under 1-sun AM1.5 using the one diode ideal model. Impact of minor carrier lifetime and surface recombination velocity in the top sub-cell on the cell performances is analyzed. Optimum composition of the top sub-cell has been identified ($x = 51.8$ % and $E_g = 1.68$ eV). The simulation results predict, for the optimized InGaN/Si double-junction solar cell, a short-circuit current $J_{sc} = 20$ mA/cm^2, an open-circuit voltage $V_{oc} = 1.97$ V, and a conversion efficiency $\eta = 38.3\%$.

1 Introduction

Multi-junction solar cells have been extensively studied in the past few years due to the limitations in the ability of one junction solar cell to utilize efficiently the photons of the broad solar spectrum. A multi-junction solar cell divides the solar spectrum into spectral ranges, each being converted in a different sub-cell, to achieve high overall conversion efficiency. A currently common approach is to arrange the sub-cells in a mechanically stacked configuration [1, 2] or a tandem system [3, 4], where the sunlight strikes the highest band gap sub-cell first and progressively hits the lower band gap sub-cells.

The main problem in tandem cells is the current and lattice mismatching between sub-cells, which reduces significantly the conversion efficiency. Mechanically stacked solar cells can overcome these issues; however, they present alternative challenges due to the complexity of integration of the various sub-cells with minimal optical loss and at minimal cost.

InGaN material has become important in the fabrication of photovoltaic devices due to its attractive features [5–16]. Among these, the following is of most interest. The first is, the energy band gap lying from 0.7 to 3.4 eV, which can absorb the full solar spectrum by a single material InGaN with different indium contents. The second is the high resistance to high-energy irradiation and temperature variations, which makes it suitable for space applications or high concentration solar cell systems.

To date, the highest efficiencies are achieved with multi-junction solar cells grown on Ge or III–V substrate [17–22]. The use of standard Si substrates would reduce the cost of high-efficiency multi-junction solar cells.

Several studies and realizations on InGaN/Si multi-junction solar cells have been reported [4, 23, 24]. However, their efficiencies are limited due to lattice mismatch between InGaN and Si which generates dislocations responsible of carrier lifetime shortening and interface recombination velocity increasing.

Because of the lattice mismatch between InGaN and Si, the impact of carrier lifetime and interface recombination velocity has to be taken into account.

Novelty in this work is that in all the analysis, the current matching is maintained which optimizes the conversion efficiency.

In this study, numerical simulations are conducted to determine the performance of current-matched InGaN/Si double-junction solar cells and estimate the optimum structure leading to high-efficiency solar cells, while taking

✉ S. Nacer
nacer_sa@yahoo.com

[1] Laboratoire LATSI, Department of Electronics, University of Blida 1, BP. 270, Blida, Algeria

Published online: 11 February 2016

into account the impact of minor carrier lifetime and surface recombination velocity in the top sub-cell.

This paper is organized as follows: In Sect. 2, theoretical model is described. In Sect. 3, simulation results of the performance of InGaN/Si double-junction solar cells are discussed. Finally, conclusions are drawn in Sect. 4.

2 Theoretical model

The structure of In_xGaN/Si double-junction solar cell is shown in Fig. 1.

In this work, calculations were all performed under 1-sun AM1.5 illumination and a temperature of 300 K using the one diode ideal model. Several simplifying assumptions were made, including no reflection losses, no series and shunt resistance losses, and ignoring tunnel junction.

The equation relating $In_xGa_{1-x}N$ band gap energy to the indium concentration x is given as

$$E_g(x) = 0.77x + 3.42(1-x) - 1.43x(1-x) \quad (1)$$

The photocurrent in the top sub-cell is given by

$$J_{ph1} = \sum_{0}^{\lambda_1} (J_{ph,n} + J_{ph,p} + J_{ph,r}) \quad (2)$$

where $J_{ph,n}$ is the electron photocurrent generated in the p-type base given by

$$J_{ph,n} = qF(\lambda)\frac{\alpha L_n}{(\alpha L_n)^2 - 1}\left[\frac{\frac{S_n L_n}{D_n} + \alpha L_n}{\frac{S_n L_n}{D_n}\sinh\frac{x_j}{L_n} + \cosh\frac{x_j}{L_n}} - \left\{\alpha L_n + \frac{\frac{S_n L_n}{D_n}\cosh\frac{x_j}{L_n} + \sinh\frac{x_j}{L_n}}{\frac{S_n L_n}{D_n}\sinh\frac{x_j}{L_n} + \cosh\frac{x_j}{L_n}}\right\} e^{-\alpha x_j}\right] \quad (3)$$

$J_{ph,p}$ is the hole photocurrent generated in the n-type emitter given by

$$J_{ph,p} = qF(\lambda)\frac{\alpha L_p}{(\alpha L_p)^2 - 1}\left[\left\{\alpha L_p - \frac{\frac{S_p L_p}{D_p}\cosh\frac{d}{L_p} + \sinh\frac{d}{L_p}}{\frac{S_p L_p}{D_p}\sinh\frac{d}{L_p} + \cosh\frac{d}{L_p}}\right\} - \left\{\frac{\alpha L_p - \frac{S_p L_p}{D_p}}{\frac{S_p L_p}{D_p}\sinh\frac{d}{L_p} + \cosh\frac{d}{L_p}}\right\} e^{-\alpha d}\right] e^{-\alpha(x_j + W)} \quad (4)$$

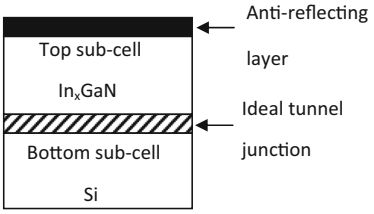

Fig. 1 Structure of InGaN/Si double-junction solar cell

$J_{ph,r}$ is the photocurrent density in the space charge region given by

$$J_{ph,r} = qF(\lambda)(e^{-\alpha x_j} - e^{-\alpha(x_j+W)}) \quad (5)$$

$F(\lambda)$ is the incident photon flux, α is the optical absorption coefficient, x_j is the junction depth, W is the width of the depletion region, d is the top sub-cell width, and $S_{n,p}$ are the surface recombination velocities.

The diffusion constants and the diffusion lengths are related by

$$L_{n,p} = \sqrt{D_{n,p}\tau_{n,p}} \quad (6)$$

where $\tau_{n,p}$ are the minority carrier lifetimes.

The absorption coefficient can be expressed as

$$\alpha(\lambda) = \alpha_0\sqrt{\frac{hc}{\lambda} - E_{g1}} \quad (7)$$

where α_0 is a constant, h is Planck's constant, c is the velocity of light, and E_{g1} is the band gap of the top sub-cell.

For bottom sub-cell, the internal quantum efficiency is considered as unit one, and the cell thickness is considered as infinite. Practically, the infinite thickness cell means that a cell with certain thickness can absorb nearly all photons with energies above its band gap.

The photocurrent of the bottom sub-cell is given by

$$J_{ph2} = \sum_{0}^{\lambda_2} qF(\lambda)e^{-\alpha d} \quad (8)$$

The limits of the summation are given by

$$\lambda_{1,2} = \frac{hc}{E_{g1,2}} \quad (9)$$

The total current of the sub-cells is given by

$$J_{1,2} = J_{ph1,2} - J_{dark1,2} \quad (10)$$

The dark current can be expressed as

$$J_{dark1,2} = J_{01,2}\left[\exp\left(\frac{qV}{kT}\right) - 1\right] \approx J_{01,2}\exp\left(\frac{qV}{kT}\right) \quad (11)$$

where V is the voltage, k is the Boltzmann constant, and J_0 is the saturation current density given by

$$J_{01,2} = qn_{i1,2}^2\left(\frac{D_n}{L_n N_A} + \frac{D_p}{L_p N_D}\right) \quad (12)$$

The intrinsic carrier concentrations are calculated from

$$n_{i1,2}^2 = N_{c1,2}N_{v1,2}\exp\left(-\frac{E_{g1,2}}{kT}\right) \quad (13)$$

where N_c and N_v are the effective densities of states given by

$$N_{c,v}(cm^{-3}) = 2.5.10^{19}\left(\frac{m^*_{n,p}}{m_0}\right)^{1.5}\left(\frac{T}{300}\right)^{1.5} \quad (14)$$

$m^*_{n,p}$ are the carrier effective masses.

From (10) and (11), the voltage of the sub-cells can be expressed as

$$V_{1,2} = \frac{kT}{q}\ln\left(\frac{J_{\mathrm{ph1,2}} - J_{1,2}}{J_{01,2}}\right) \quad (15)$$

For the tandem, the sub-cells are in series, so the voltage is the sum of the sub-cell voltages, and the current in the sub-cells is the same

$$V = V_1 + V_2 \quad (16)$$

and

$$J_1 = J_2 = J \quad (17)$$

If the current matching condition is satisfied, then

$$J_{ph1} = J_{ph2} = j_{ph} \quad (18)$$

and

$$V = \frac{kT}{q}\ln\frac{(J_{\mathrm{ph}} - J)^2}{J_{01}J_{02}} \quad (19)$$

The characteristic current–voltage of the tandem is given by

$$J = J_{\mathrm{ph}} - \sqrt{J_{01}J_{02}}\exp\left(\frac{qV}{2kT}\right) \quad (20)$$

The short-circuit current is given by

$$J_{\mathrm{sc}} = J_{\mathrm{ph}} \quad (21)$$

The open-circuit voltage of a tandem cell is taken to be equal to the sum of the open-circuit voltage of the sub-cells

$$V_{\mathrm{oc}} = V_{\mathrm{oc1}} + V_{\mathrm{oc2}} \quad (22)$$

The open-circuit voltage of the sub-cells is given by

$$V_{\mathrm{oc1,2}} = \frac{kT}{q}\ln\left(\frac{J_{\mathrm{ph1,2}}}{J_{01,2}} + 1\right) \quad (23)$$

The maximum power $P_{\max}$ that the cell can produce is calculated by finding the voltage and the current that maximize the product $J.V$, found by setting its derivative equal to zero.

$$\left(\frac{\mathrm{d}(J.V)}{\mathrm{d}V}\right) = 0 \quad (24)$$

The efficiency of the tandem cell is given by

$$\eta = \frac{P_{\max}}{P_{\mathrm{in}}} \quad (25)$$

where P_{in} is the total input power.

The procedure adopted in our calculations is as follows

- The composition (x) and the band gap of the top sub-cell satisfying the current matching conditions are calculated by

$$J_{\mathrm{ph1}}(x) = J_{\mathrm{ph2}}(x) \quad (26)$$

- The short-circuit current, the open-circuit voltage V_{oc}, and the conversion efficiency η are then calculated.

3 Results and discussions

The junction depth x_j of the top sub-cell is set to 0.1 μm, the doping of the top-cell regions is $N_A = N_D = 10^{18}$ - cm^{-3} and the parameters of InGaN are obtained by linear interpolation of those of the binaries InN and GaN. The parameters of the binaries used in the simulations are reported in Table 1.

3.1 InGaN band gap and absorption coefficient

Figure 2 shows the variation of the band gap E_{g1} of In_x-$Ga_{1-x}N$ as a function of indium concentration. It can be seen that E_{g1} decreases when increasing indium concentration. It can also be seen that when varying indium concentration, E_{g1} can be tuned from 0.77 to 3.4 eV,

Table 1 Parameters of the binaries used in the simulations

Semiconductor	E_{g} (eV)	m^*_n	m^*_p	D_n (cm^2/s)	D_p (cm^2/s)
Si	1.12	0.98	0.49	39	12
InN	0.77	0.11	1.63	80	8
GaN	3.42	0.2	0.8	39	0.75

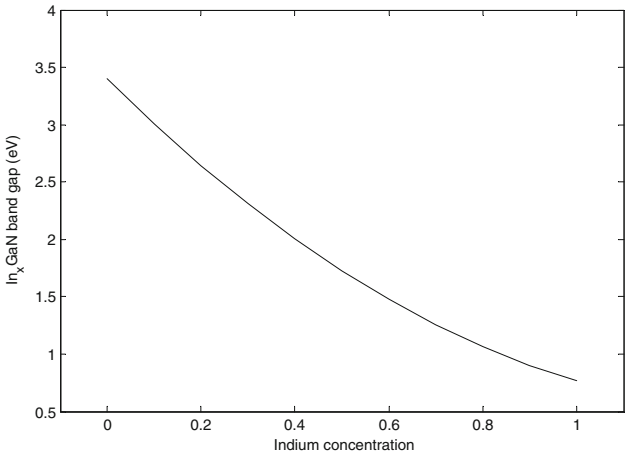

Fig. 2 Variation of the band gap of InGaN as a function of Indium concentration

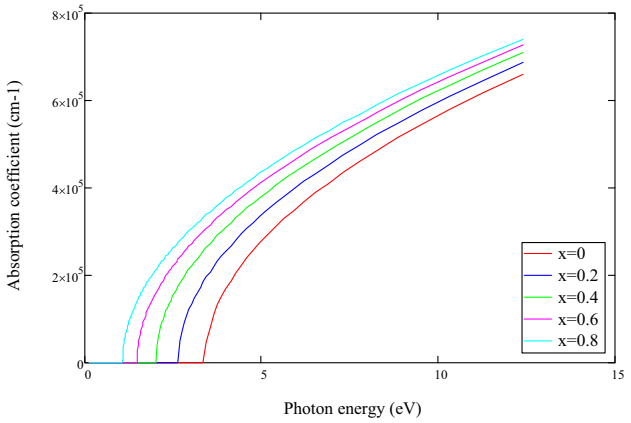

Fig. 3 Variation of the InGaN absorption coefficient as a function of the photon energy for different indium concentrations

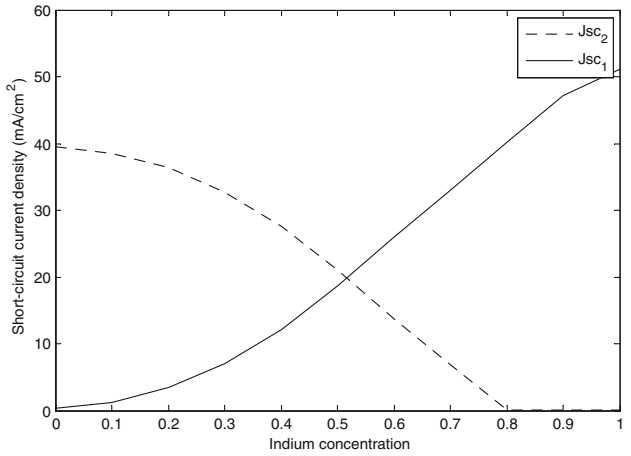

Fig. 4 Variation of the short-circuit currents of the sub-cells tandem as a function of Indium concentration ($d = 1$ µm, $\tau_n = \tau_p = 10$ ns, $S_n = S_p = 10^3$ cm/s)

covering nearly the whole solar spectrum. Figure 3 represents the variation of the InGaN absorption coefficient as a function of the photon energy for different indium concentrations.

3.2 Current matching

In a multi-junction cell, one of the most important design criteria is to achieve the current matching between the sub-cells. Current matching enables us to optimize the conversion efficiency.

The variation of the short-circuit currents in the sub-cells as function of indium concentration is represented in Fig. 4, for a top-cell thickness fixed to $d = 1$ µm, a carrier lifetime $\tau = \tau_n = \tau_p = 10$ ns, and a surface recombination velocity $S = S_n = S_p = 10^3$ cm/s. When the indium concentration increases, the band gap of the top sub-cell decreases leading to broaden the absorbed spectrum, so the short-circuit current J_{sc1} increases, whereas the transmitted spectrum to the bottom sub-cell is reduced, and thus its short-circuit current J_{sc2} decreases. It can also be noticed that the current matching is obtained for an indium concentration $x = 51.8$ % corresponding to a band gap $E_g = 1.68$ eV. Figure 5 shows the indium concentration and the top-cell thickness d required to realize the current matching condition between the sub-cells. It can be seen that for a thickness d greater than 1 µm, the indium concentration tends toward a constant value $x = 0.518$. This is because, at this width, nearly all the photons with energy above the band gap E_{g1} are absorbed, and the short-circuit current J_{sc1} saturates.

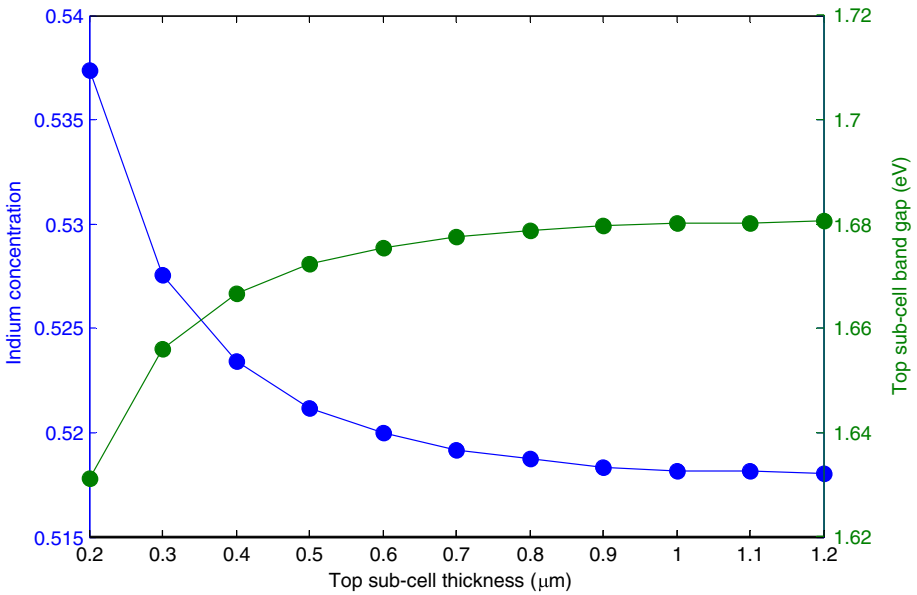

Fig. 5 Indium concentration and top-cell thickness d required to realize the current matching condition ($\tau_n = \tau_p = 10$ ns, $S_n = S_p = 10^3$ cm/s)

3.3 Impact of minority carrier lifetime

The minority carrier lifetime is one of the most critical parameters in determining the efficiency of a solar cell. Defects and dislocations generated at the III–V/Si hetero-interface may serve as recombination centers and decrease the minority carrier lifetime. We simulated the effect that lower lifetimes would have on device performance for a fixed top sub-cell $d = 1$ μm and a surface recombination velocity $S = 10^3$ cm/s. For each value of the carrier lifetime τ, the compositions x and the band gap E_{g1} satisfying the current matching condition are determined. Then for these values, the short-circuit current, the open-circuit voltage, and the conversion efficiency are calculated. Figure 6 shows the effect of carrier lifetime ($\tau = \tau_n = \tau_p$) on the indium concentration required to maintain the current matching. Figure 7 shows the impact of the carrier lifetime on the short-circuit current. It can be seen that J_{sc} starts to degrade for $\tau < 10$ ns, due to the recombination of carriers before reaching the junction. Figure 8 shows the impact of the carrier lifetime on the open-circuit voltage of the top sub-cell. V_{oc1} decreases when decreasing the minority

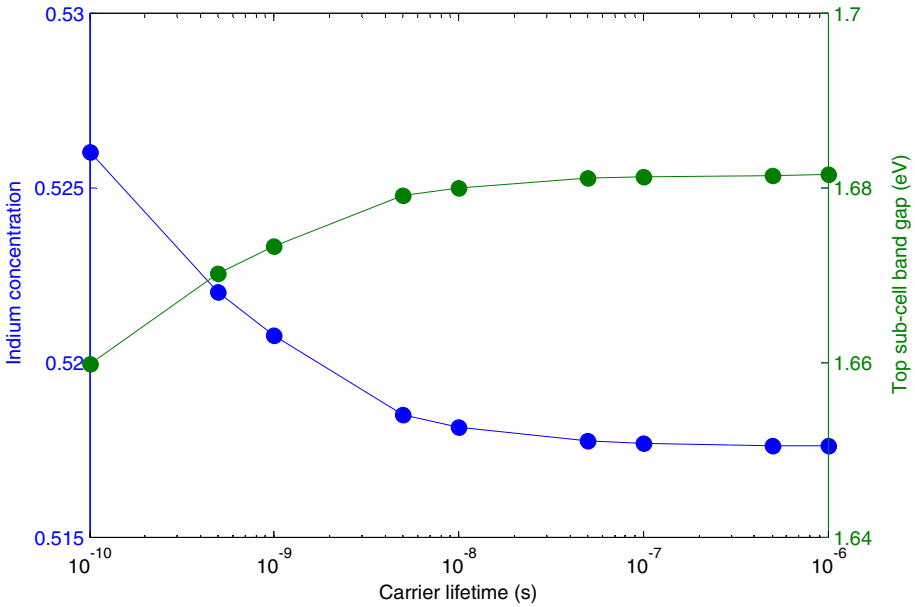

Fig. 6 Effect of carrier lifetime on the Indium concentration required to maintain current matching ($d = 1$ μm, $S_n = S_p = 10^3$ cm/s)

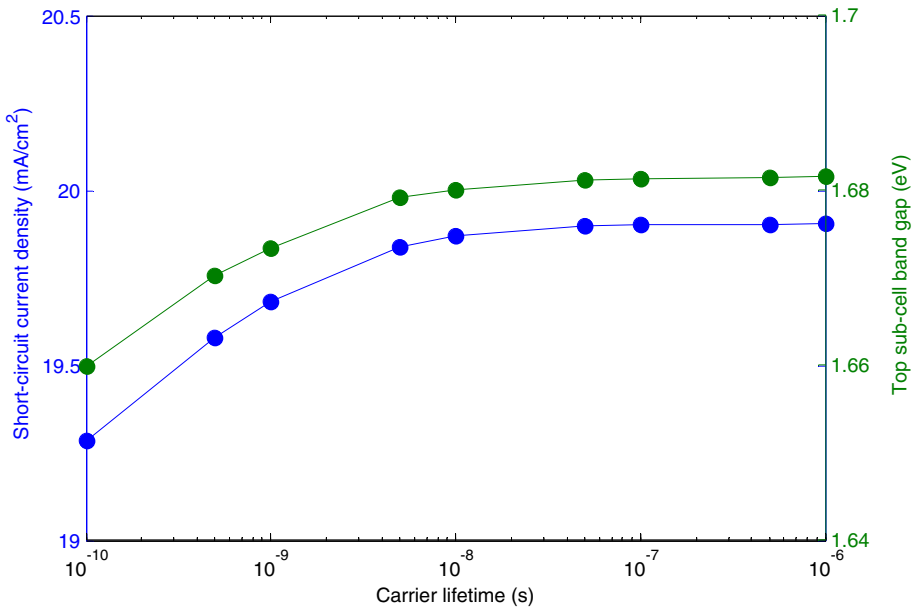

Fig. 7 Impact of the carrier lifetime on the top-cell short-circuit current ($d = 1$ μm, $S_n = S_p = 10^3$ cm/s)

carrier lifetime. This degradation is attributed to the reverse saturation current density J_0 which is inversely proportional to the minority carrier lifetime. Figure 9 shows the impact of the carrier lifetime on the conversion efficiency of the 2J InGaN/Si cell. It can be seen that with increasing the carrier lifetime, the efficiency increases. Efficiency higher than 38 % can be attained for lifetime greater than 10 ns. However, the efficiency degrades significantly for $\tau < 10$ ns due to the reduction in both J_{sc} and V_{oc}, as seen earlier.

3.4 Impact of surface recombination velocity

Surface and interface recombination velocity of the top sub-cell ($S = S_n = S_p$) could be a major factor that limits the performance of the tandem cell. We simulated the effect that higher surface recombination velocity would have on device performance for a fixed top sub-cell $d = 1$ µm and a carrier lifetime $\tau = 10$ ns. In all the analysis, the current matching is maintained. Figure 10 shows the effect of S on the indium concentration required

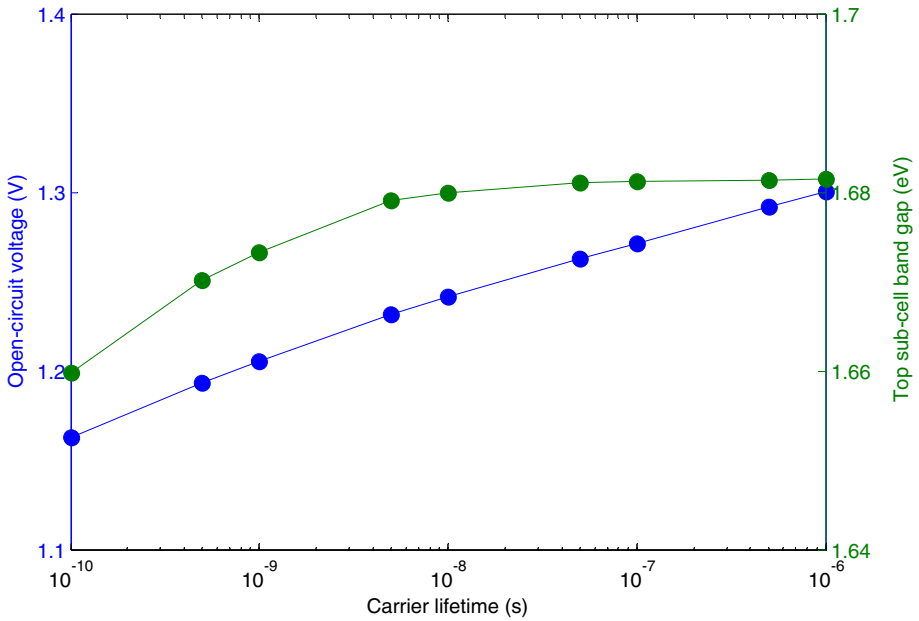

Fig. 8 Impact of the carrier lifetime on the open-circuit voltage of the top sub-cell ($d = 1$ µm, $S_n = S_p = 10^3$ cm/s)

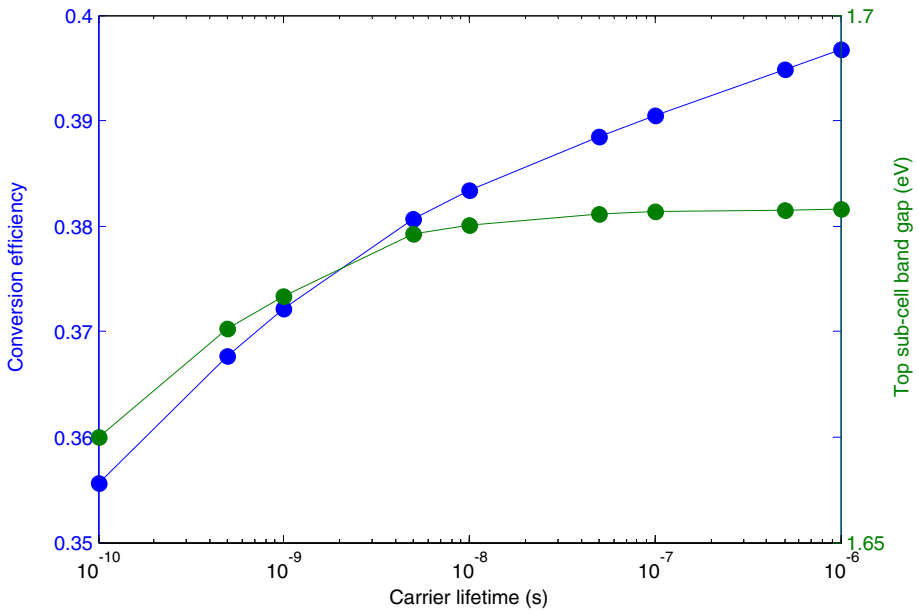

Fig. 9 Impact of the carrier lifetime on the conversion efficiency of the 2J InGaN/Si cell ($d = 1$ µm, $S_n = S_p = 10^3$ cm/s)

to maintain the current matching. In Fig. 11 is shown the impact of S on the short-circuit current. It can be seen that J_{sc} starts to degrade for $S > 10^3$ cm/s, due to the recombination of carriers at the interface. Figure 12 shows the impact of S on the open-circuit voltage. V_{oc1} starts to degrade significantly for $S > 10^3$ cm/s. This degradation is attributed to the reduction in the short-circuit current. Figure 13 shows the impact of S on the conversion efficiency of the 2J InGaN/Si cell. It can be seen that efficiency as high as 38 % can be attained for S lower than 10^3 cm/s. However, the efficiency degrades significantly for $S > 10^3$ cm/s due to the reduction in both J_{sc} and V_{oc}, as seen earlier.

3.5 Temperature dependence of InGaN/Si solar cell parameters

As the temperature has a great impact on the solar cell operation, we have studied the variation of solar cell parameters versus the temperature. Figure. 14 shows the variations of the open-circuit voltage and the conversion efficiency as a function of the temperature. The tempera-

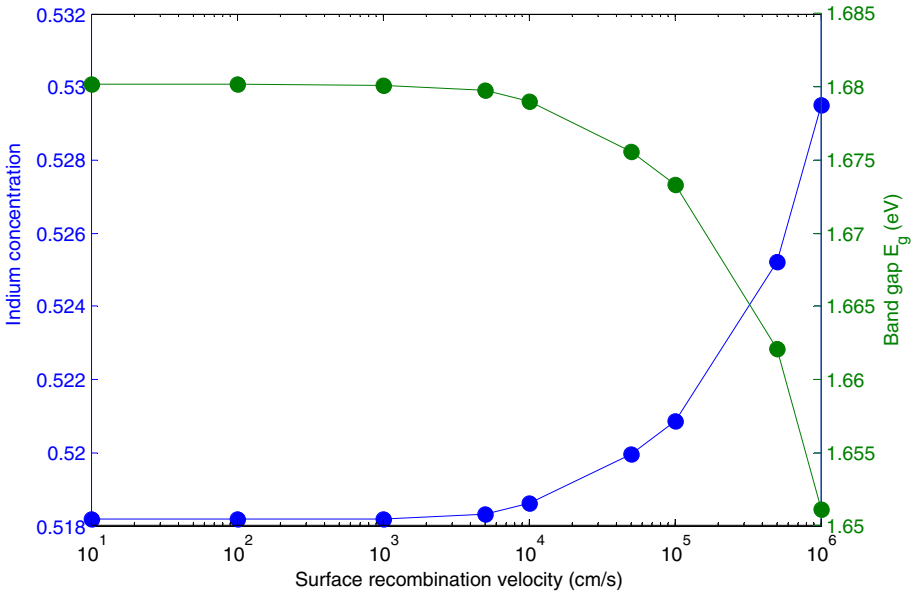

Fig. 10 Effect of surface recombination velocity on the Indium concentration required to maintain current matching ($d = 1$ µm, $\tau = 10$ ns)

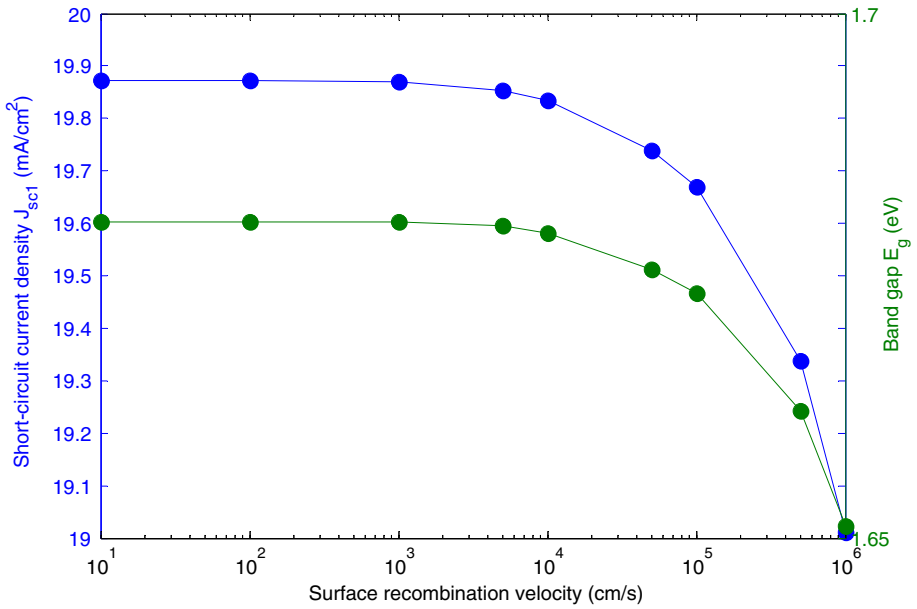

Fig. 11 Impact of surface recombination velocity on the short-circuit current ($d = 1$ µm, $\tau = 10$ ns)

ture was varied from 300 to 400 K, and the temperature dependence of the band gap was ignored. As can be seen, the open-circuit voltage decreases strongly, inducing the degradation of the conversion efficiency. The high reduction in the open-circuit voltage with the increased temperature is caused by the increase in the reverse saturation current density due to the exponential dependence of the intrinsic carrier concentration with the temperature (Eq. 13). Therefore, good heat sinking of such cells is necessary for maintaining a high-energy conversion efficiency when using concentration.

Figure 15 shows the current–voltage (J–V) curve of the optimized InGaN/Si double-junction solar cell ($x = 51.8$ %, $E_g = 1.68$ eV, $d = 1$ µm, $\tau = 10$ ns, $S = 10^3$ cm/s and $T = 300$ K) exhibiting a short-circuit current of 20 mA/cm^2, an open-circuit voltage of 1.97 V, and a conversion efficiency of 38.3 %.

Some published results of InGaN double-junction solar cell conversion efficiency are summarized in Table 2. In Ref. [27], the high value of the efficiency corresponds to the limit conversion efficiency of a tandem (1.1/1.68 eV) where ideal cells are considered.

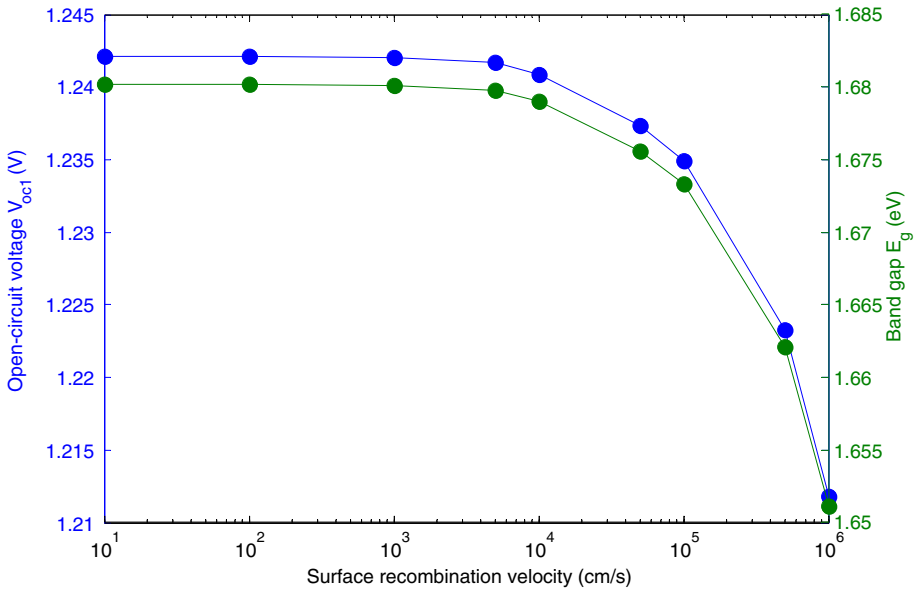

Fig. 12 Impact of surface recombination velocity on the top-cell open-circuit voltage ($d = 1$ µm, $\tau = 10$ ns)

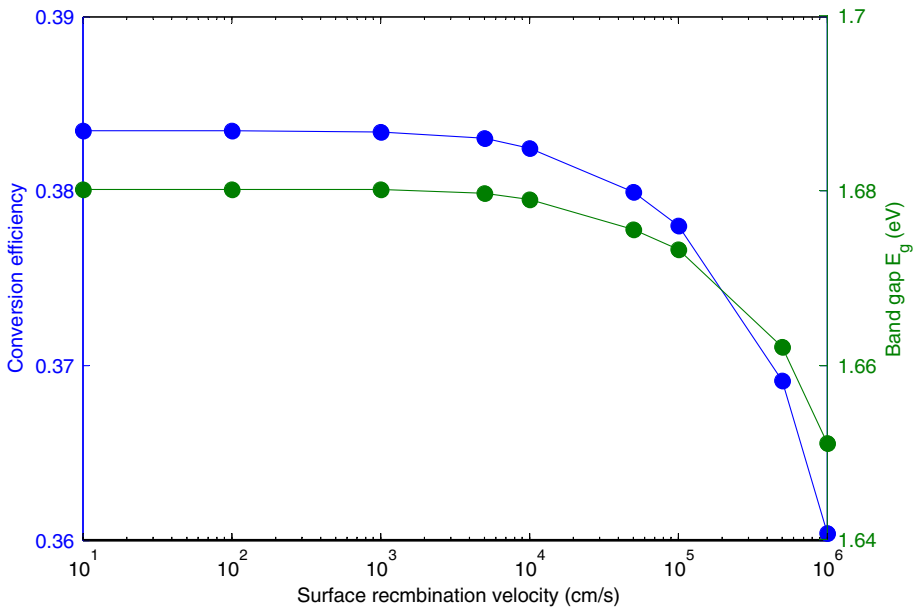

Fig. 13 Impact of surface recombination velocity on the conversion efficiency of the 2J InGaN/Si cell ($d = 1$ µm, $\tau = 10$ ns)

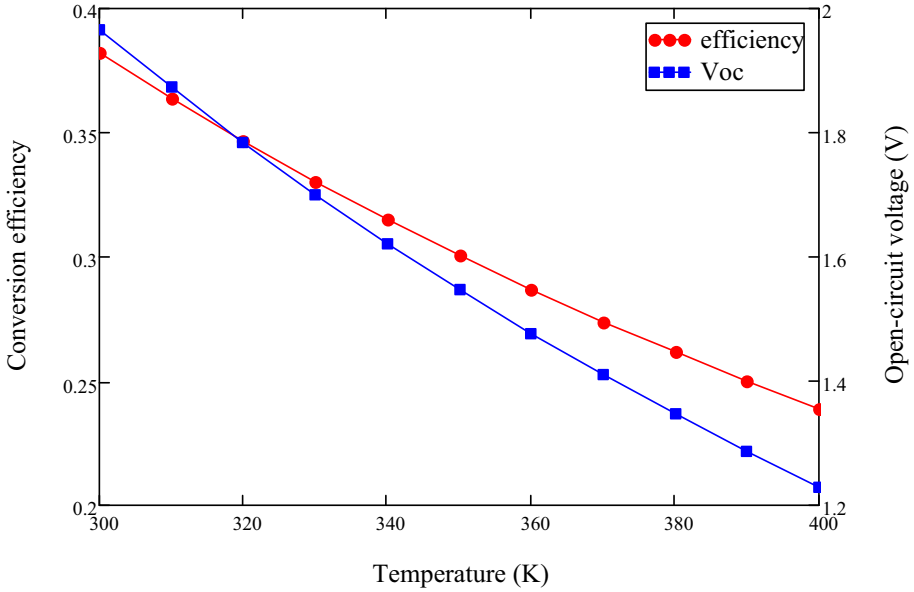

Fig. 14 Variations of the open-circuit voltage and the conversion efficiency as a function of the temperature ($x = 51.8$ %, $E_g = 1.68$ eV, $d = 1$ µm, $\tau = 10$ ns and $S = 10^3$ cm/s)

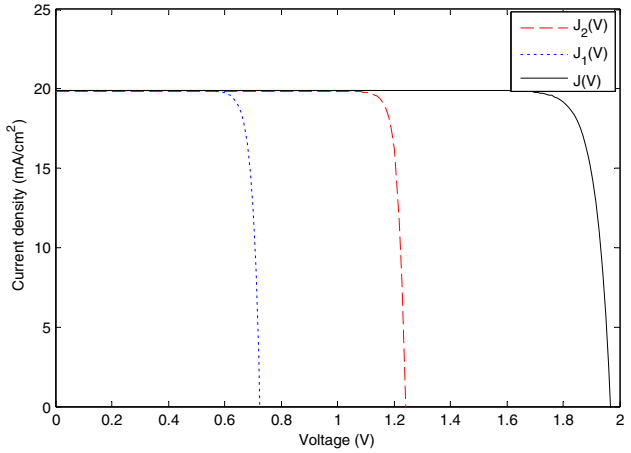

Fig. 15 Current–voltage curve of the optimized InGaN/Si double-junction solar cell ($x = 51.8$ %, $E_g = 1.68$ eV, $d = 1$ µm, $\tau = 10$ ns, $S = 10^3$ cm/s and $T = 300$ K)

Table 2 Published results of InGaN double-junction solar cell conversion efficiency

Structure	Conversion efficiency (%)	References
InGaN/InGaN	34.7	[26]
InGaN/InGaN	35.1	[25]
InGaN/InGaN	27.49	[3]
InGaN/Si	36.5	[24]
InGaN/Si	31	[4]
InGaN/Si	35.2	[2]
InGaN/Si	38.3	This work
1.68 eV/1.1 eV	44	[27]

4 Conclusion

The theoretical design and optimization of InGaN/Si double-junction solar cells for high efficiency have been studied using the one diode ideal model. The optimum composition of the top sub-cell ensuring current matching has been identified. The simulation results predict for the optimized InGaN/Si double-junction solar cell a short-circuit current $J_{sc} = 20$ mA/cm^2, an open-circuit voltage $V_{oc} = 1.97$ V, and a conversion efficiency $\eta = 38.3$ %. Adding a second InGaN junction with an appropriate alloy composition can provide further boost to the efficiency. All these results suggest that the InGaN alloy is an excellent candidate for high-performance and low-cost solar cells.

References

1. S. Yoshidomi, J. Furukawa, M. Hasumi, T. Sameshima, Mechanical stacking multi-junction solar cells using transparent conductive adhesive. Energy Procedia **60**, 116–122 (2014)
2. Z. Li, H. Xiao, X. Wang et al., Theoretical simulations of InGaN/Si mechanically stacked two-junction solar cell. Phys. B Condens. Matter **414**, 110–114 (2013)
3. H. Hamzaoui, A.S. Bouazzi, B. Rezig, Theoretical possibilities of $In_xGa_{1-x}N$ tandem PV structures. Sol. Energy Mater. Sol. Cells **87**, 595–603 (2005)
4. L. Hsu, W. Walukiewicz, Modeling of InGaN/Si tandem solar cells. J. Appl. Phys. **104**, 024507 (2008)
5. A.G. Bhuiyan, K. Sugita, A. Hashimoto, A. Yamamoto, InGaN solar cells: present state of the art and important challenges. IEEE J. Photovolt. **2**(3), 276–293 (2012)
6. B.R. Jampana, A.G. Melton, M. Jamil, N. Faleev, R.L. Opila, I.T. Ferguson, C.B. Honsberg, Design and realization of wide band gap (~2.67 eV) InGaN p–n junction solar cell. IEEE Electron Device Lett. **31**(1), 32–34 (2010)

7. X. Zhang, X. Wang, H. Xiao, C. Yang, J. Ran, C. Wang, Q. Hou, J. Li, Simulation of $In_{0.65}Ga_{0.35}N$ single-junction solar cell. J. Phys. **40**(23), 7335–7338 (2007)
8. S. Feng, C.M. Lai, C.Y. Tsai, Y.R. Su, L.W. Tu, Modeling of InGaN p–n junction solar cells. Opt. Mater. Express **3**(10), 1777–1788 (2013)
9. S.W. Feng, C.M. Lai, C.H. Chen, W.C. Sun, L.W. Tu, Theoretical simulations of theeffects of the indium content, thickness, and defect density of the i-layer on the performance of p-i-n InGaN single homojunction solar cells. J. Appl. Phys. **108**(9), 093118 (2010)
10. M.-J. Jeng, Simulation of nonpolar p-GaN/i-$In_xGa_{1-x}N$/n-GaN solar cells. Int J Photoenergy **2012**, 910256 (2012). doi:10.1155/2012/910256
11. M. Nawaz, A. Ahmad, A TCAD-based modelling of GaN/InGaN/Si solar cells. Semicond. Sci. Technol. **27**, 035019 (2012)
12. M.-H. Wu, S-P. Chang, S.-J. Chang, R.-H. Horng, W.-Y. Liao, R.-M. Lin. Characteristics of GaN/InGaN double-heterostructure photovoltaic cells. Int J Photoenergy **2012**, 206174 (2012). doi:10.1155/2012/206174
13. X. Cai, Y. Wang, B. Chen, M.M. Liang, W.J. Liu, J.Y. Zhang, X.Q. Lv, L.Y. Ying, B.P. Zhang, Investigation of InGaN p-i-n homojunction and heterojunction solar cells. IEEE Photnics Tech. Lett. **25**(1), 59–62 (2013)
14. O. Jani, I. Fergusaon, C. Honsberg, S. Kurtz, Design and characterization of GaN/InGaN solar cells. Appl. Phys. Lett. **91**(13), 132117 (2007)
15. J.R. Lang, C.J. Neufeld, C.A. Humi, S.C. Cruz, E. Matioli, U.K. Mishra, J.S. Speeck, High external quantum efficiency and fill-factor InGaN/GaN heterojunction solar cells grown by NH_3-based molecular beam epitaxy. Appl. Phys. Lett. **98**(13), 131115 (2011)
16. X.M. Cai, S.W. Zeng, B.P. Zhang, Fabrication and characterization of InGaN p-i-n homojunction solar cell. Appl. Phys. Lett. **95**(17), 173504 (2009)
17. R.R. King, D.C. Law, K.M. Edmondson, C.M. Fetzer, G.S. Kinsey, H. Yoon, R.A. Sherif, N.H. Karam, 40% efficient metamorphic GaInP/GaInAs/Ge multijunction solar Cells. Appl. Phys. Lett. **90**, 183516 (2007)
18. J.M. Olson, S.R. Kurtz, A.E. Kibbler, P.A. Faine, 27.3-percent efficient Ga0.5In0.5P/GaAs tandem solar-cell. Appl. Phys. Lett. **56**, 623–625 (1990)
19. K.A. Bertness, S.R. Kurtz, D.J. Friedman, A.E. Kibbler, C. Kramer, J.M. Olson, 29.5-percent-efficient GaInP/GaAs tandem solar-cells. Appl. Phys. Lett. **65**, 989–991 (1994)
20. T. Takamoto, E. Ikeda, H. Kurita, M. Ohmori, Over 30% efficient InGaP/GaAs tandem solar cells. Appl. Phys. Lett. **70**, 381–383 (1997)
21. L.M. Fraas, J.E. Avery, V.S. Sundaram, V.T. Kinh, T.M. Davenport, J.W. Yerkes, J.M. Gee, K.A. Emery, Over 35% efficient GaAs/GaSb stacked concentrator cell assemblies for terrestrial applications. In Proceedings of the 21st IEEE Photovoltaic Specialists Conference, Kissimimee, FL, USA, (May 1990), pp. 190–195
22. M.S. Leite, R.L. Woo, J.N. Munday, W.D. Hong, S. Mesropian, D.C. Law, H.A. Atwater, Towards an optimized all lattice-matched InAlAs/InGaAsP/InGaAs multi-junction solar cell with efficiency >50%. Appl. Phys. Lett. **102**, 033901 (2013)
23. I. Mathews, D. O'Mahony, B. Corbett, A.P. Morrison, Theoretical performance of multi-junction solar cells combining III-V and Si materials. Opt. Express **20**, A754 (2012)
24. S.W. Feng, C.M. Lai, C.Y. Tsai, L.W. Tu, Numerical simulation of the current-matching effect and operation mechanisms on the performance of InGaN/Si tandem cells. Nanoscale Res. Lett. **9**, 652 (2014)
25. X. Zhang et al., Theoretical design and performance of $In_xGa_{1-x}N$ two-junction solar cells. J. Phys. D Appl. Phys. **41**, 245104 (2008)
26. S. Nacer, A. Aissat, Simulation and optimization of current matching multi-junction InGaN solar cells. Opt. Quantum Electron. **47**, 3863–3870 (2015)
27. Henning Doscher et al., Epitaxial III–V films and surfaces for photoelectrocatalysis. ChemPhysChem **13**(12), 2899 (2012)